RSC Advances

ROYAL SOCIETY OF CHEMISTRY

www.rsc.org/advances

Cite this: DOI: 10.1039/c0xx00000x

www.rsc.org/xxxxxx

ARTICLE TYPE

A New Single/Few-layered Graphene Oxide with Giant Dielectric Constant of 10^6: Contribution of defects and functional groups

K. Santhosh Kumar[a], Suresh Pittala[c], Srinath Sanyadanam[c] and Pradip Paik*[a,b]

Received (in XXX, XXX) XthXXXXXXXXX 20XX, Accepted Xth XXXXXXXXX 20XX

DOI: 10.1039/b000000x

Herein this work we introduce single/few layered graphene oxide (GO) synthesized with ultrasonication and demonstrate the colossal dielectric permittivity in the frequency range 20 Hz to 2 MHz and in 30 to 180^{o}C temperature range. A giant dielectric constant of GO (~10^6) with low loss has been observed at 1 KHz and at 30^{0}C which is even very high compared to the conventional dielectric materials such as $CaCu_3Ti_4O_{12}$. The conductivity of our GO has been calculated and found to be 3.980 x 10^{-5}-1.943 x 10^{-5} (DC) and 2.0 x 10^{-3}-1.7x10^{-2} (AC). The various conducting mechanisms which can govern the conductivity (AC and DC) of the GO with the varying frequency and temperature have been discussed using impedance spectroscopy. The mechanistic approach and the role of functional groups, defects, temperature and frequency have been elucidated which lead to the high dielectric constant. The variation of activation energy from 1.15 (1KHz) to 0.58 (2.0MHz) is related to the frequency dependent conductivity of the л-л conjugated electrons and their hopping has also been discussed. Present dielectric results are superior compared to the GOL (with less defects/less time sonicated). Present finding directed that the new GO can be used for scaling advances high performance electronic devices and high dielectric based electronic and energy storage devices.

1. Introduction

Dielectrics are the materials which have wide range of applications such as for fabricating microelectronic for large scale power applications and energy storage devices.[1] Dielectric materials with high permittivity and low losses are used in the capacitors to store more electrical energy.[2] For metal, relative permittivity is negative and charge placed on the surface dissipates faster whereas for dielectrics it is positive and charge placed on the surface dissipates slowly. The materials with colossal permittivity for use in capacitor meet the limited success. However, because of the evolution of high dielectric constant materials like $ATiO_3$-type perovskite titanates (where, A = Ca, Sr, Ba, Pb or their solid solution),[3] a large amount of electrical charge storage is possible through capacitors. The discovery of giant dielectric constant of 10^5 in $CaCu_3Ti_4O_{12}$ (or equivalently $Ca_{1/4}Cu_{3/4}TiO_3$) is very recent and this value is very high compared with the ferroelectric materials (1000-50,000).[4–6] Addition to that $CaCu_3Ti_4O_{12}$ without any dopants show very strong nonlinear current-voltage (I-V)characteristics.[7] In principle, a substantial lattice vibrations displaced the intrinsic dipole moment and yield a very high dielectric permittivity which could be explained by the Lyddane-Sachs-Teller model.[8] However, many other theoretical studies[9,10]and experimental works[11–14]have been performed to explain such a giant dielectric constant. Nevertheless, several factors such as morphology, contribution of grain boundaries, internal material layers etc. are the reasons for the giant high dielectric properties. Another reason for the high dielectric phenomenon is the extrinsic effects such as the interfacial polarization of highly delocalized electrons at the grain boundaries.[1] Hu and co-workers[15] have shown that doping of electron acceptors such as In^{3+} with addition of co-dopant Nb^{5+} into rutile lower the dielectric losses due to the stoichiometric local lattice defects (defect clusters due to the conversion of Ti^{+4} to Ti^{+3}) and are responsible for the extraordinarily high value of intrinsic value of permittivity over most of the radio frequency ranges.

Graphene Oxide (GO) is a monolayer of Graphite Oxide which consists of hydroxyl, and epoxide functional groups on the basal plane and carbonyl and carboxyl groups attached at the edges of the sheet.[16,17]In the recent years GO has been synthesized by variety of methods and GO is less conducting in nature.[18] It can be used as dielectric material in various applications. Reduced graphene oxide (r-GO) films were used to grow cells and showed enormous biocompatibility.[19] Films formed of r-GO have shown potential even in solar cells.[20] Few reports on the dielectric study of GO/graphene based materials composites exist in the literature to increase the dielectric properties of host materials,[21]andgraphene based materials.[22] Recently, MnO_2 decorated graphene nanoribbons showed superior permittivity and excellent microwave shielding properties.[23]*S. Ruoffet al.* showed that chlorinated r-GO can enhance the dielectric constant of r-GO/Polymer composites.[24] The low dielectric constant and ultrahigh strength graphene oxide/polyimide composite films were also reported.[25]Verdejo*et al.* showed that the homogeneous dispersion of GO through out the polymer matrix can effectively increase the dielectric permittivity.[26]Graphene-poly(vinylidene fluoride)composites with multi-layered structure prepared by a solution-cast and hot-pressing showed a large dielectric constant as high as 7940 after percolation threshold.[27] In this work we have synthesize GO through sonochemical approaches and studied the dielectric dispersion of pellet of single/few layers GO

without adding of any dopants and represents the colossal dielectric for its use in various applications. The remarkably new synthesis approach of GO makes it as a new competing materials and allow the use as a colossal permittivity materials and permit scaling advances in electronic devices. Finally, we demonstrate the mechanisms for high dielectric phenomena and relaxation of GO in detail and compared the results with less defective GO and rGO..

2. Experimental Section

2.1 Synthesis of Graphene oxide (GO):

GO was synthesized followed by modified Hummer's method from natural graphite powder with a high power ultrasonication. In brief,3 g of graphite powder was added into a solution at80°Cthat consists of con.H_2SO_4 (97 wt%, 12 ml), $K_2S_2O_8$ (2.5 g), and P_2O_5 (2.5 g). The temperature of the mixture was maintained at 80°C for 6h. Then the mixture was diluted at RT with 0.5L of DI water and then left it for 12 hrs. To remove the residual acid, the mixture was filtered and washed with de-ionized water. The product was dried at ambient conditions for 12 hrs. Further oxidation of pre-oxidized graphite was performed as follow.1 g of partially-oxidized graphite was taken and $NaNO_3$ (0.5 g) was added in a flask. Then, con.H_2SO_4 (97 wt%, 25 ml) was added under stirring at ice cooled condition. Then $KMnO_4$ (3g) was added to this mixture for 1 hr in many steps. Stirring and ice-cooled condition were maintained for another2 hrs. Afterword it was stirred for 2 days. Then dil.H_2SO_4 (aqueous solution, (5 wt %, 100 ml) was added slowly maintaining bath temperature 98°C. The stirring was continued for another 2 hrs at 98°C. The resultant mixture was cooled to 60°C.Then H_2O_2 (30 wt% in water, 3 ml) was added drop wise under ultrasonication foranother2 hrs at 35°C. Then the oxidized product was purified by rinsing with dil. HCl solution (10 wt% to H_2O) repeatedly. Purification process was performed by repeated washing, centrifugation and redispersion using DI water. Finally, the product was dried through freeze drying.

2.2 Fabrication of GO pellet for dielectric measurements:

100 mg GO powder was taken and pressed into a pellet using 8 mm stainless steel dye and carver Wabash hydraulic press. The load (3 tonnes for 1 minute) was optimized to get the maximum density of pellet (1.42 gm. cm^{-3}) and to measure it's dielectric behavior. After making the pellet, it was kept in the vacuum desiccator and later in a globe box so that no moisture is absorbed. Before taking Dielectric measurements, proper electroding was assured using silver conducting paste (Cat. No. 735825, SIGMA-ALDRICH**)** on both the sides of the pellet in glove box and dried it at 45°C for 24 hr in a vacuum chamber to remove all the volatile material from the conducting paste, and dielectric measurements were conducted within the electromagnetic frequency range(20 Hz to 2 MHz). The dimension of the resultant palette is measured to be 8.0 mm in diameter and 3.0 mm in thickness at the maximum density.

2.3 Characterizations

High resolution scanning electron microscopy (HRSEM) (Model: HITACHI S-3400 N), field emission SEM (Model: ULTRATM 55 UK ZEISS) and High resolution transmission electron microscopy (HRTEM) (Model: FEI TECHNAI G2 200 kV S-twin) were performed to find out the shape, size and morphology of the GO. The 3D topography surface properties and layer structure was confirmed by the noncontact mode of AFM (SII Oo Seiko Instruments Inc.). Elemental analysis was performed with an energy dispersive X-ray spectroscopy (EDS) (HORIBA 7021H). FTIR-active characteristics were found out by the Fourier transform infra-red (FT-IR) (Nicolet model Impact-410) studies. GO powder has been mixed with dry KBr by grinding in an agate mortar followed by making pellets using hydraulic press with a load of 9 tones which is melting load of KBr. A pellet with 10 mm diameter was made and kept in the FTIR instrument and spectrum has been collected after making required background elimination. UV-Vis-NIR experiments were conducted with a LAMDA 750 spectrometer (PerkinElmer). XPS were conducted with an Omicron Nanotechnology XPS system, (X-ray source: Al Kα, 1486.6 eV). Thermogravimetry analysis (TGA) measurements were performed with a Thermo ONIX Gaslab 300 TGA instrument from 30–1000°C in an N_2 atmosphere with a heating rate of 10°C/min. Raman spectra for GO and Graphite powder were recorded with a Witech Alpha 200 Confocal Raman spectrophotometer. 532nm Nd YAG Laser, 2nd harmonic was used as excitation source, focused to a 2 µm spot size.

3. Results and Discussion

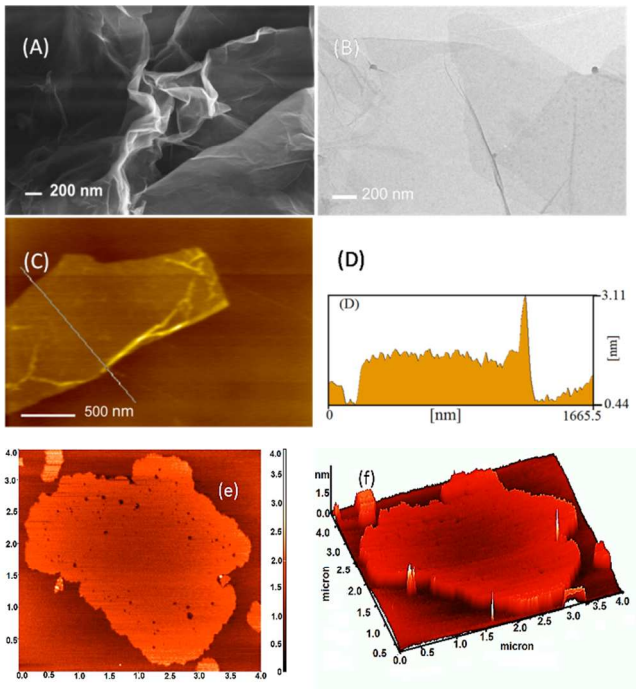

Figure 1.(a) FESEM micrograph (b) TEM micrograph (c) AFM Topography image (d) Surface line profile of GO obtained from AFM. (e) and (f) showing the 2D and 3D images of GO, respectively having defects (black spots).

Figure 1(a) shows the high resolution FESEM image of the GO taken at 80 KX magnification and 5.5 mm working distance. Operating voltage is 5 KV. The GO sheets present in this image are transparent in nature, which indicates the very low thickness. Mono layer graphene/GOis electron transparent.[28] Energy dispersive spectra (EDS) of the GO sample was taken at 15 KV accelerating voltage and the corresponding spectra are shown in Figure S1 (a) and (b) (supporting file). The Figure S1 (supporting file) is clearly referring for the existence of the carbon and oxygen in the GO sheets. No other peaks are present and that means our sample is pure GO. At the same time even though hydrogen atom is present, it can't be detected by the SEM detector.

From TEM, Figure 1(b) it can be noticed that GO is electron transparent.[28] The transparency of GO depends on the number of layers associated with it. As the number of layers increases, transparency decreases.[28] In Figure 1(b) few areas observed that are not electron transparent and may be due to the folded edge of more number of a GO sheet associated together. And also uniformity in the electron transparency indicates most of the image area consists of mono layer GO sheet. The continuation of these sheets indicates that their lateral size is more than few micrometers. AFM is the best technique to find out the thickness/height profile of the graphene or GO layers. For this work twenty numbers of the AFM topography images of the GO sample were taken to find out the thickness of the GO sheet and the number of layers present. The Figure 1(c) shows the AFM semi-contact mode topography image of GO. The line marked across the flake is for obtaining the surface height profile of the GO sheet through the inbuilt software of AFM instrument. The corresponding height profile is shown in Figure 1(d). From the height profile the maximum height (z-height) along that line is found to be around 1.33 nm and indicates that it is a bi or maximum a tri-layered GO sheet. That to if we carefully observe the height profile, it is not uniform. That is it is flat almost entire region. But only at the end of the sheet the sudden increase in the height profile is observed. From this we can say that at the edge of the monolayer GO there is a part of other layer corrugated or it is folded. Further to scrutiny the defects on the GO surface more AFM experiments have been performed and the representative 2D and 3D images are showing in Figure 1 (e) and (f), respectively. The black spots on the surface of Figure 1 (e) and (f) are the defects. The surface height profile with respect to the Figures 1(e) and (f) has been provided in the supporting file (Supporting Figure S1(c)) .

To know the chemical functionality of the synthesized GO FTIR has been performed. Figure 2(a) shows the FTIR spectrum of GO powder sample which consists of peaks as follows. The peak appeared at 1236 cm^{-1} is due to the C-O (epoxy) bond, 1397 cm^{-1} for C-O (carboxyl), 1586 cm^{-1} for C=C peak, 1718 cm^{-1} for C=O peak, 2357 cm^{-1} peak attributed to the stretching of O-C=O. The peak at 2929 cm^{-1} for is C-H stretching and 3420 cm^{-1} is for the O-H peak. No other peaks are appeared in the spectrum. Hence, our sample is a pure GO powder.

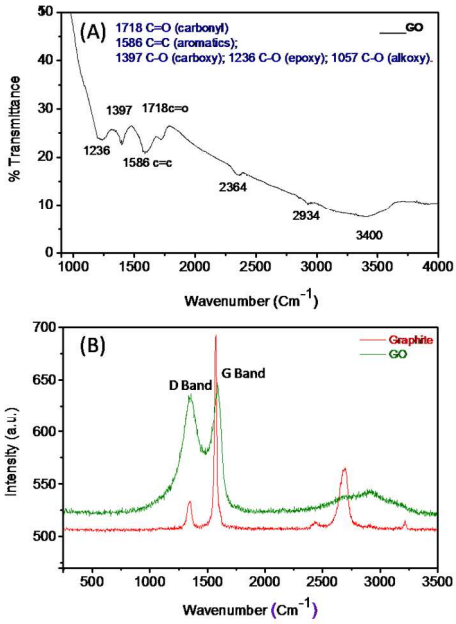

Figure 2. (a) FTIR spectrum of GO (b) Raman spectrum of GO and pristine natural graphite.

Raman spectroscopy is a powerful non-destructive tool to characterize the carbonaceous materials, particularly for distinguishing ordered and disordered crystal structures of carbon. The typical features for carbon in Raman spectra are the G line around 1582 cm^{-1} and the D line around 1350 cm^{-1}. The G line is usually assigned to the E_{2g} phonon bands of C sp^2 atoms, while the D line is a breathing mode of κ-point phonons bands of $A1_g$ symmetry.[29,30] The overtone of the D line, the D′ line, is located at 2700 cm^{-1}, while the G′ line (the overtone of the G line) is around 3248 cm^{-1}. Figure 2(b) shows the Raman spectra of pristine graphite and GO nano sheets. The Raman spectrum of the pristine natural graphite displays a strong G band at 1582 cm^{-1}, a weak D band at 1350 cm^{-1}, a broad D′ line at 2690 cm^{-1}, and a very weak G′ line at 3245 cm^{-1}. In the Raman spectrum of GO nano sheets, the G band is broadened and shifted right to 1595 cm^{-1}. At the same time, the intensity of the D band at 1350 cm^{-1} increases substantially. These phenomena could be attributed to the significant decrease of the size of the in-plane sp^2 hybridized domains due to the oxidation and ultrasonic exfoliation, and partially ordered graphite crystal structure of graphene nanosheets.[31] To check the purity and water content in the sample we performed TGA (Figure 3) and observed that the slight variation of weight at 100 °C is attributed to the loss of free moisture. The abrupt weight loss around 200 °C is due to the pyrolysis of the oxygen-containing functional groups, generating CO, CO_2 and water vapour[32]. And the weight loss after 200 °C is due to the continuous degradation of remaining –COOH and –OH groups..

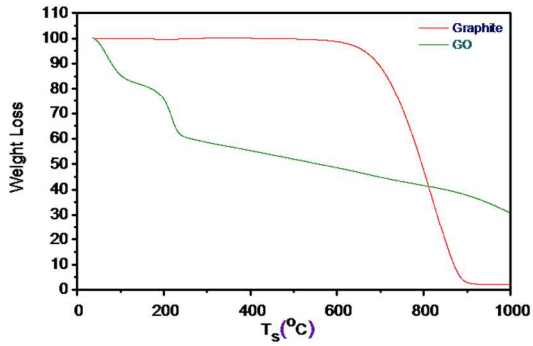

Figure 3. Shows TGA thermogram of graphite and GO with a heating rate of 5°C per minute in N_2 atmosphere.

XPS is a surface sensitive technique which gives atomic contents and also local chemical environment of the elements present up to few nanometers in the GO surface. The XPS survey scan and high resolution spectra of corresponding elements of GO have been shown in Figure 4. The survey scan (Figure 4(a)) shows the existence of two sharp peaks which corresponds to carbon and oxygen elements. The high resolution XPS spectrum of C 1s shown in Figure 4(b),which is deconvoluted and peaks at 284.9, 287 and 288.8 eV confirm for the presence of C-C, C=O and O=C-OH functional groups, respectively.[33] Figure 4(c) shows the O 1s high resolution XPS spectrum which is having two prominent peaks at 531.1 and 532.7 eV. These peaks are attributed to the presence of O=C-OH and C=O oxygen containing groups in GO,respectively.[33]

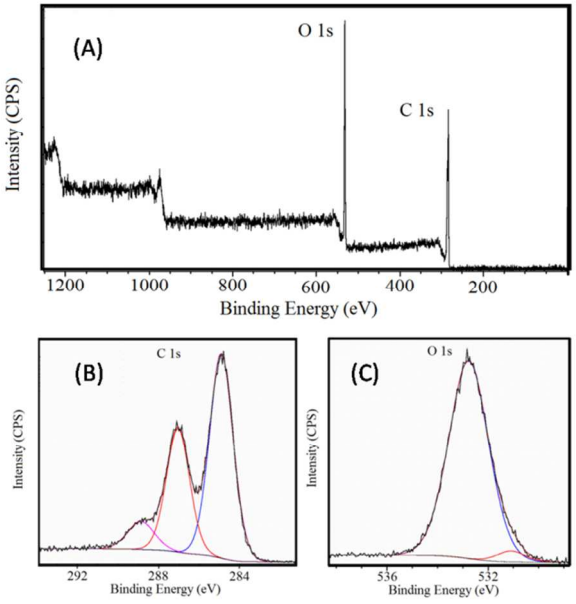

Figure 4. Shows XPS survey spectrum of GO(a) High resolution XPS spectrum of (b) C 1s (C) O 1s

The dielectric measurements were conducted for the sample under study to know its relaxation behavior. Measurements were

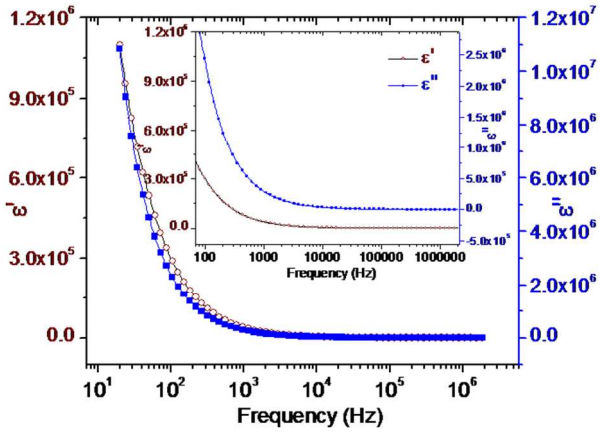

Figure 5. Shows the real and imaginary parts of dielectric constant of GO with frequency (shown from 20 Hz) at room temperature.

conducted with varying frequency and temperature. The frequency dependence of the real part of the dielectric constant (ε′) and the imaginary part of the dielectric constant (ε′′) is depicted in the Figure 5. The in-set of Figure 5 is the magnified plot for lower values of ε′ and ε′′. It is observed that ε′ and ε′′ are showing similar behavior with the frequency. The sudden fall in the values of ε′and ε′′are observed at low frequencies, whereas ε′ and ε′′decrease slowly at the higher frequency region. At lower frequency range let say at 1 kHz the value of dielectric constant is very high and in the order of $1.05x10^6$. From Figure 5, it is also evident that the dielectric constant is ranging from $3.0x10^5$-$1x10^6$ in the frequency range of1 kHz-5 kHz. As the frequency increases the dielectric constant reaches to a value of 648 even at 1 MHz. In general, for all materials, the dielectric constant continuously decreases with frequency. Because as the frequency increases, some of the contributions to the dielectric constant such as ionic, orientation, space-charge dies out at different frequency ranges and hence reduces the ε′ value. Also dipoles can't orient with the high applied alternating field and thus results in dielectric loss. In the present case, very high ε′ value at low frequency is observed and the ε′ value at high frequency is might be due to the change in orientational polarization of functional groups (e.g., -OH, and --COOH) present on the surface of the GO basal plane. The relaxation behaviour is also shown in the Figure 5. This relaxation is showing similar in nature as the ε′shows with the frequency.

Further, the dielectric behavior of GO has also been studied with varying temperature (30-180°C) at a particular frequency, since its start to lose weight beyond 200°C. Figure 6 shows a comparison of dielectric behavior of GO sample at various constant frequencies with the increase in temperature. We observe that the value of ε′ is decreasing with the increase infrequency. At 30°C temperature, the dielectric constant for 1 KHz is ~35000 and with increase in temperature initially it increases to ~40000 (100°C) and then decreases to ~20000 (180°C) due to the thermal vibration of chemical bonds as well as due to the change in the dipole moment and orientation polarization of the functional groups (-OH and –COOH). Similar trend is also observed for all other frequencies in the same temperature domain. However, with increase in the frequency the

dipoles can't orient at high applied alternating field and at higher temperature and subsequently results in the dielectric losses (Figure 6(a) and 6(b)). At higher temperature GO loses its thermal stability due to the degradation and loss of moisture CO, and CO_2 due to the thermal degradation of functional groups(-OH and –COOH) (See TGA results, Figure 3, Figure S11 and S12) and this is an expected common frequency dependent dielectric phenomenon of almost all the insulating thermally low stable dielectric materials.

There may be an obvious question, why the dielectric constant of GO initially increases with temperature for a particular frequency? The reason is that, at a constant frequency, as the temperature increases a sudden increase in the dielectric constant has observed due to the reorientation/rearrangement of polarization of the functional groups present in the GO and transition observed is due to the loss of absorbed moisture (TGA, Figure 3). Further, the orientation/rearrangement of the attached functional groups (-OH and -COOH) present in the basal plan of GO are resulted low dielectric constant at higher temperature and frequency.

The dispersion of dielectric constant as a function of frequency has been studied[34,35] at various temperatures (30-180°C) and results are shown in Figure 7. From Figure 7 it is apparent that the dielectric constant is very high at the low frequency range and it decreases as the frequency increases. This is due to the ceasing of the contributions of different polarizations with increase in the frequency. As shown in Figure 7, this high value at low frequencies is observed due to the interfacial polarization and the consequent decrease is observed due to non-cope up of the molecular dipoles with alternating fields. The effects of temperature on dielectric constant of GO are also clearly seen in Figure 7. As the temperature increases the initial dielectric constant value also decreases at lower frequencies. Higher temperature is causing in the thermal fluctuations/change of mode of bond vibrations at intermolecular distance as well as dipoles which restrict them to orient in the direction of the applied electric field.

The dispersion of dielectric constant with temperature has been studied and the temperature dependence of ionic conductivity has been investigated by plotting ln(σ) *vs*. (1/T) at different frequencies and is shown in Figure 8. All the plots demonstrate the Arrhenius type of behavior. By calculating the slope of respective plots the values for activation energy (E_a) have been calculated and presented in Table 1.

As the temperature increases the conductivity likewise increases for all the plots irrespective to the frequency. This is owing to the hopping of ions/л-electrons through the conjugated basal plane along the -C=C- bonds of GO. There might be some atomic (carbon) vacancies/defects that may exist on the basal plane of GO sheet like graphene [36,37] which can lead to the transportation of charges/ions which in general happens in many ionic solid conductors e.g., NaCl. The effect of frequency on ionic

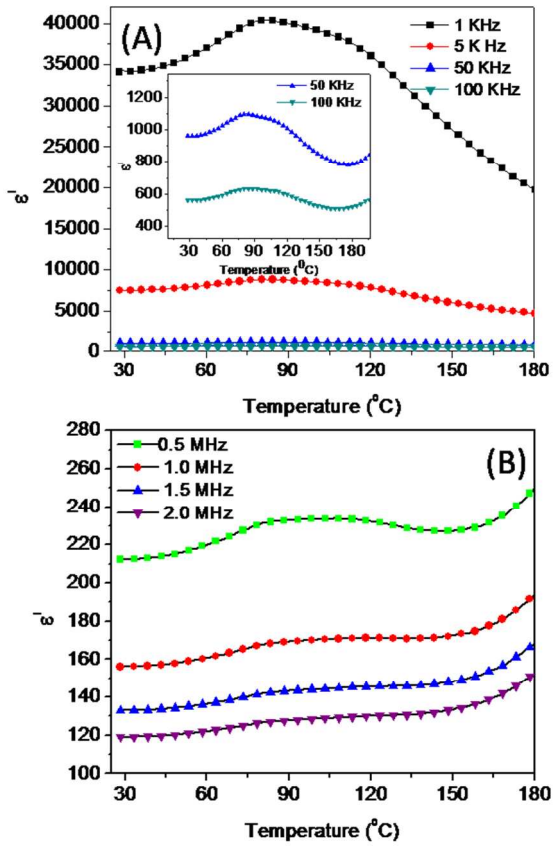

Figure 6. Shows the dielectric dispersion of GO (a) for 1, 5, 50 and 100 KHz (b) for 0.5, 1.0, 1.5 and 2 MHz with increase in temperature.

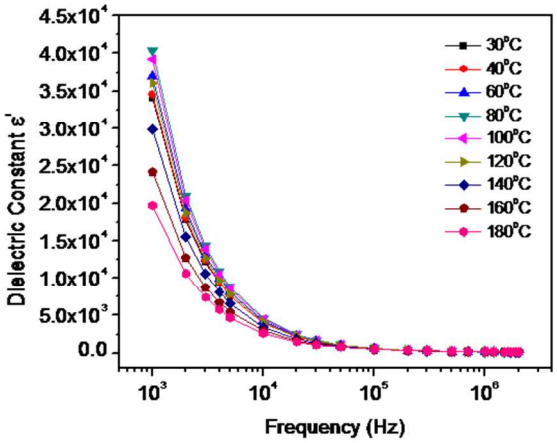

Figure 7. Shows the dielectric dispersion of GO with frequency (shown from 10^3Hz) at different temperatures.

Table 1.Shows the variation in activation energy with frequency of GO.

Sl.No.	Frequency (KHz)	Activation Energy (E_a), eV
1	1	1.15
2	5	0.78
3	50	0.88
4	500	0.64
5	1000	0.64
6	1500	0.59
7	2000	0.58

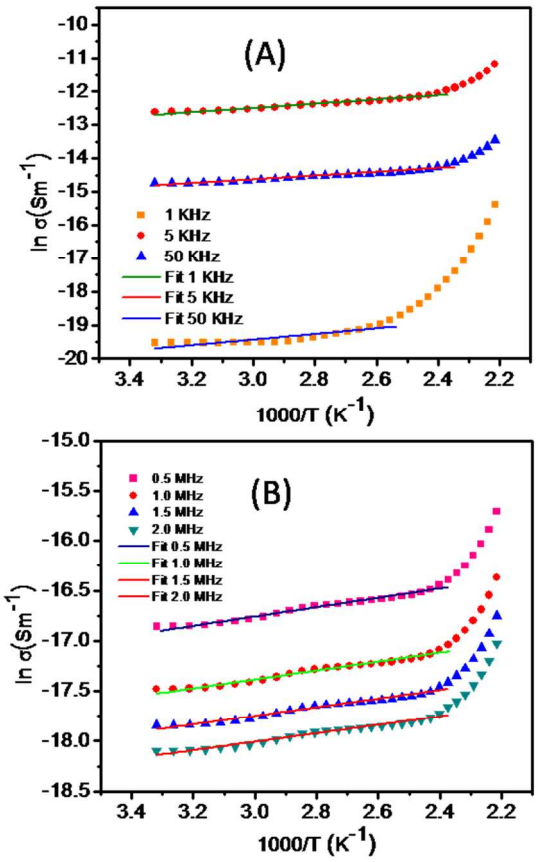

Figure 8.Shows log (σ) versus 1/T plots and fitted curves of GO sample at (A) 1 KHz, 5 KHz and 50 KHz (B) 0.5 MHz, 1.0 MHz, 1.5 MHz and 2 MHz frequencies.

conductivity is also prominent for GO (Figure 8 (b)) which reveals that the ionic conductivity is less at higher frequencies and follows the similar trend as the temperature increases. At lower temperature range the molecular dipoles of GO due to the presence of the polar groups –OH and –COOH can easily be re-oriented conferring to the alternating field mechanism and henceforth the ionic conduction values are less.

From Figure 9 (A), it is manifested that the dielectric loss (Tan δ) is decreasing with the frequency. The reason for this is, as the frequency increases the dipoles cannot orient along direction of the applied electric field, and thus the loss due to moment of the charges are decreased. If we compare all the plots at different temperatures, loss is high at high temperature. This is due to the high thermal agitation/vibration of dipoles on the GO basal plane. However, for all the frequency the loss is in between 2-5 up to 80°C. As the temperature decreases, the thermal agitation/vibration decreases and the loss is less. From Figure 9(B), it is clear that as the temperature increases loss also increases irrespective to the frequency.

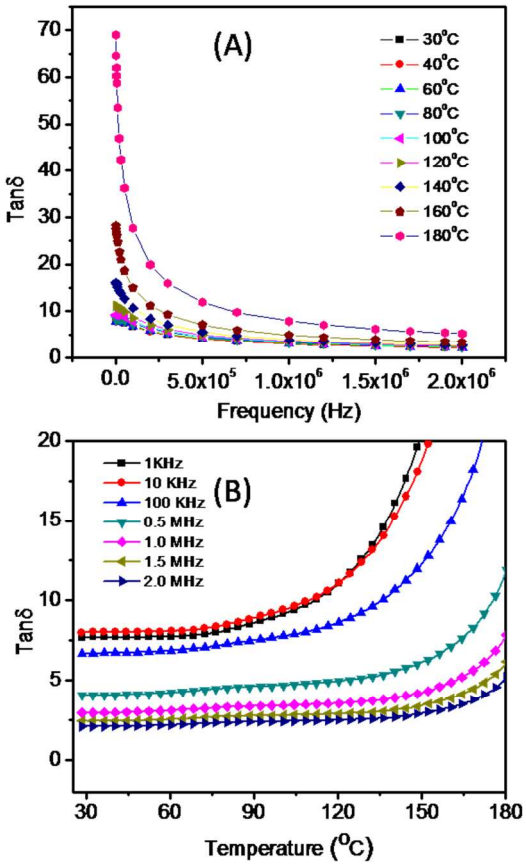

Figure 9. Shows plots of frequency versus Tanδ at various temperatures (A), and temperature versus Tanδ at various frequencies (B) of GO sample.

The impedance measurements have been executed for the GO sample after making it into pellet as it has been mentioned in the experimental section. Impedance has been recorded at different temperatures by varying frequency.

The corresponding plot between real part (Z′) and imaginary parts of impedance (Z′′) is shown in Figure 10 as a representative plot obtained at RT. Plots for other temperatures have been shown in supporting Figure (Figure S3 to Figure S11). The plots are showing a combination of two semi circles indicating contribution from basal planes and the attached functional groups of GO. Since it is not poly-crystalline material therefore the grain and grain boundary contributions are not applicable here.

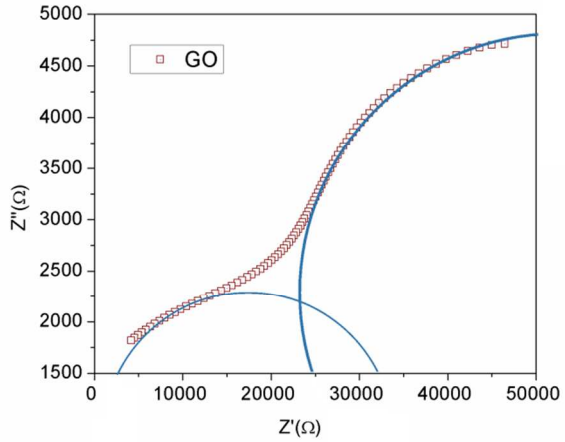

Figure 10. Shows the Cole-Cole plot of GO sample at RT and fitted curves (solid blue lines).

Table 2.The d.c. conductivity values of GO sample obtained by Cole-Cole analysis at various temperatures.

Sl.No.	Temperature in ^{o}C	R_o Value from Cole-Cole analysis in Ω	DC Conductivity σ_{DC} (Ω-m)
1	20	25091	$3.980X10^{-5}$
	40	24665	$4.05X10^{-5}$
3	60	22628	$4.419X10^{-5}$
4	80	21506	$4.640X10^{-5}$
5	100	22661	$4.412X10^{-5}$
6	120	26514	$3.771X10^{-5}$
7	140	30768	$3.250X10^{-5}$
8	160	39279	$2.245X10^{-5}$
9	180	51465	$1.943X10^{-5}$

The data is fitted to obtain various parameters using the following Cole-Cole equation (1):

$$Z = Z\infty + \frac{(Zo - Z\infty)}{[1+(i\omega\tau)^{\alpha}]} \quad (1)$$

Where, z_o, z_∞ are static impedance and impedance at high frequency, respectively; ω is the angular frequency, τ is the average relaxation time and α is the angle of semicircle arc. The obtained d.c. conductivity values from the Cole-Cole analysis[38] were calculated and shown in Table 2.

The Cole-Cole plots and corresponding fittings at each temperature have been shown in the supporting information (Figure S3 to Figure S11). The obtained d.c. conductivity values are plotted against the temperature values and shown in Figure 11(a). From Figure 11(a) it can be seen that d.c. conductivity initially increases up to 80^{o}C and then decreases till 180^{o}C.

The A.C. conductivity σ_{ac} as a function of frequency has been calculated using the following equation and the plots are shown in the Figure 11(b).

$$\sigma_{AC} = \left[\frac{Z\prime}{(Z')^2+(Z'')^2}\right] * (t/A) \quad (2)$$

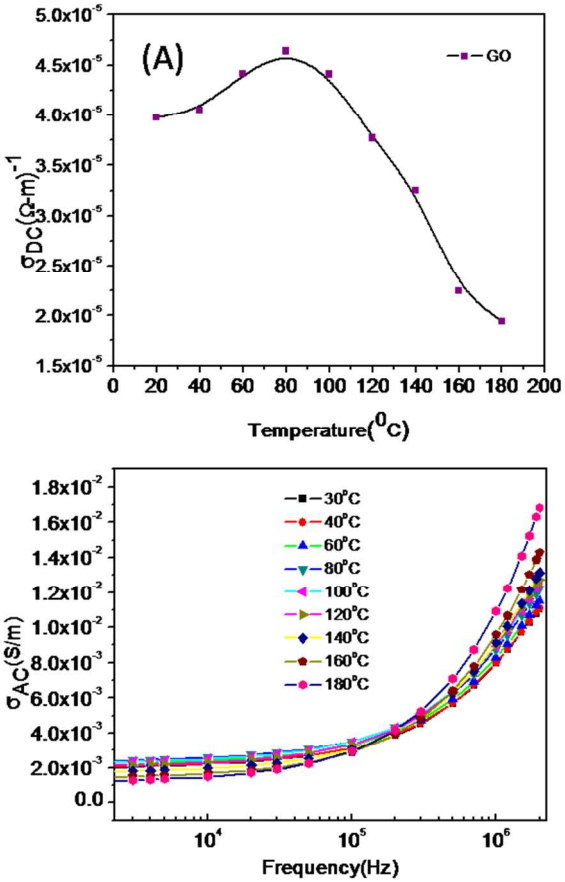

Figure 11. DC conductivity with varying temperature (a) and AC conductivity with varying frequency at particular temperatures (b) of GO sample.

Z' and Z'' are the real and the imaginary parts of impedance, t is the thickness and A is the area of the sample. There is no much variation in the A.C. conductivity in the low frequency region is observed but at higher frequencies there is one order magnitude change in the conductivity for every 10^{o} C increase in temperature observed. At 2 MHz , for all the measurements the A.C conductivity is observed to be 1.8 x 10^{-2} S/m, whereas it is 2 x 10^{-3} S/m at 20 Hz. There is also a minor variation in the conductivity with temperature. As the temperature increases the increase in the A.C. conductivity is observed. At 180^{o}C, as mentioned earlier pyrolysis of GO occurs and GO converted partially into rGO/graphene sheet as the result of degradation of the functional groups.[39] So, a number of the sp^3 hybridized basal functionalized carbon atoms converted into the sp^2 hybridized carbons and therefore the л-electron system is ultimately changing. This conversion of $sp^3 \rightarrow sp^2$ is predominantly occurred at the defective sites of the GO because numerous simulations indicate that –OH, -COOH or other functional groups can easily attached to the vacancy-type defect sites of a graphene/graphite sheet (Schematic 1-3)[40,41] along with the oxidation at the defect free sites (Schematic 1(a) →(d) conversion for defect free site

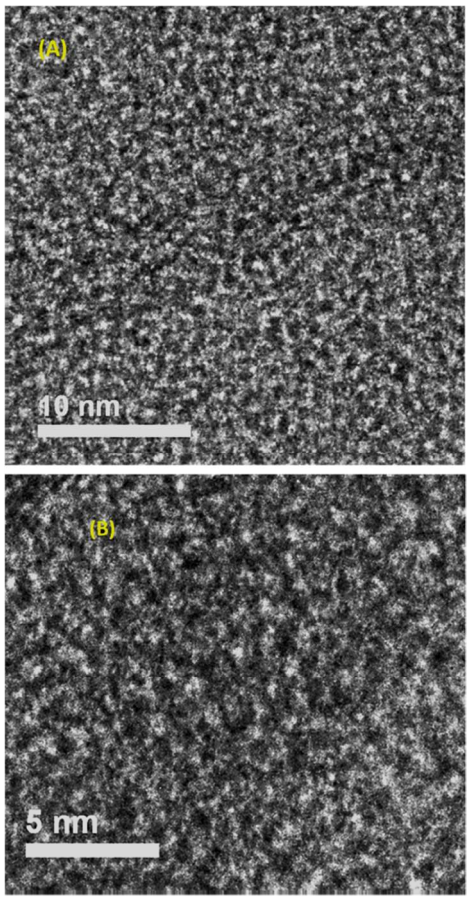

Figure 12. (a) and (b)HRTEM images of GO at low and high magnification, respectively. The white spots are the oxidized region of the sheet.

oxidation) since, at the vacancy site the л-electron density as well as the reactivity are more and energetically favourable for oxidation.[40,42,43] Now there is a question whether there is any contribution of defects for the colossal dielectric value of GO or not? Answer is yes, but how? To find out the defect status of the GO sheet we performed the HRTEM. The HRTEM micrograph (Figure 12) shows that the nature of the defects of GO is similar to the graphene/surface of graphite,[44] which are mostly non-hexagonal ring type bonding geometry (white spots in the Figure 12 are the functional groups).[28]

We have oxidized the micron sized graphite sheet into 1-2 layered GO in presence of required chemicals using highenergy ultra sounds (20 KHz), however there is a possibility of formation of non-hexagonal ring type defects by reconstruction of graphitic lattice/graphene as like as Stone-Wales (SW)[45–47] types of defect (55-77 type) which further converted into the oxide form (GO), since the required defect formation energy is few eV only(See schematic representation, Figure 13(b)→(e) conversion), and is energetically favourable state.[47] Whereas we can assume that the single vacancy (SV) defects are forming in GO is due to the removal of atom from the lattice position by high energy ultra sound which we have used during the synthesis of GO and energetically favourable for the oxidation figure 13(Figure 13 (c)→(f) conversion), because the SV formation requires very less energy (E_f~1.3 eV).[48,49] In the vacancy site there will be a change in the polarization on application of electric field which contributed to the high dielectric properties. Furthermore, in the honeycomb lattice system of graphitic sheet when we apply the ultra sound there is a possibility of formation of SV defects which under goes a John-Teller type of distortion, in which the system go into a lower energy state and form a non-degenerate energy state[50,51] and this leads to the saturation of two dangling bonds out of three towards the missing atom. Under this condition another dangling bond contribute to the high dielectric permittivity of GO along with the contribution of functional groups which are attached at the defect sites. Moreover, we cannot expect the existence of 3d defects in GO since it is only one-two layers of carbon sheets (only 0.7 nm thick). Apart from this there is a possibility of defects like one dimensional line defects as well as presence of defects at the edge of the GO layer where the carbon atoms and the free hydrogen atoms are dangling as shown in figure 14(Figure14 (a)). Furthermore, different types of reconstructions of graphite layers at the edges are possible as shown in figure 14(b) and (c)). All these defects are very prone to chemical oxidations. These oxide forms of GO as shown in Figures 14 (d), (e) and (f), and these also contribute to the change in the polarization as well as to the dielectric permittivity. Further we cannot avoid the formation of defects in the bilayer GO. Bilayer GO consists of stacked two monolayers (from the thickness of the AFM results, Figure 1 (c)). Similar to the graphite the inter layer distance between adjacent bilayer GO is approximately 3.35Å which is directed by the weak van der Waals forces of interactions between the adjacent GO layers and the defects can present in both the layers. Again we cannot avoid the formation of covalent inter layer bonds during the formation of GO when the adatoms are located between the bi-layers/adjacent layers.[52] These covalent inter layer bonds lead to the creation of Frenkel-pair (adatom-vacancy complex) in one layer and change the hybridization of the adjacent layer so that opposite carbon atoms from the two layers get connected (bridging of bonds) *via* one extra carbon atoms.[52] Such defects are also important for change in the polarization of the GO and add the value for the high dielectric constant. Many other different types of defects can be present in GO like graphene Figure 15 which can cause the disturbance of the electron transport/delocalization and responsible for the colossal dielectric permittivity for the GO.[36] Due to the defective GO basal plane and due to the Sp^2–Sp^3 conversion after functionalization with –OH, -COOH etc. л→л transition of electrons are restricted and hence decreases the conductivity of GO compared to the graphene/or few layered graphene and as a result increase the dielectric constant. In conclusion, the obtained dielectric constant

Cite this: DOI: 10.1039/c0xx00000x

www.rsc.org/xxxxxx

ARTICLE TYPE

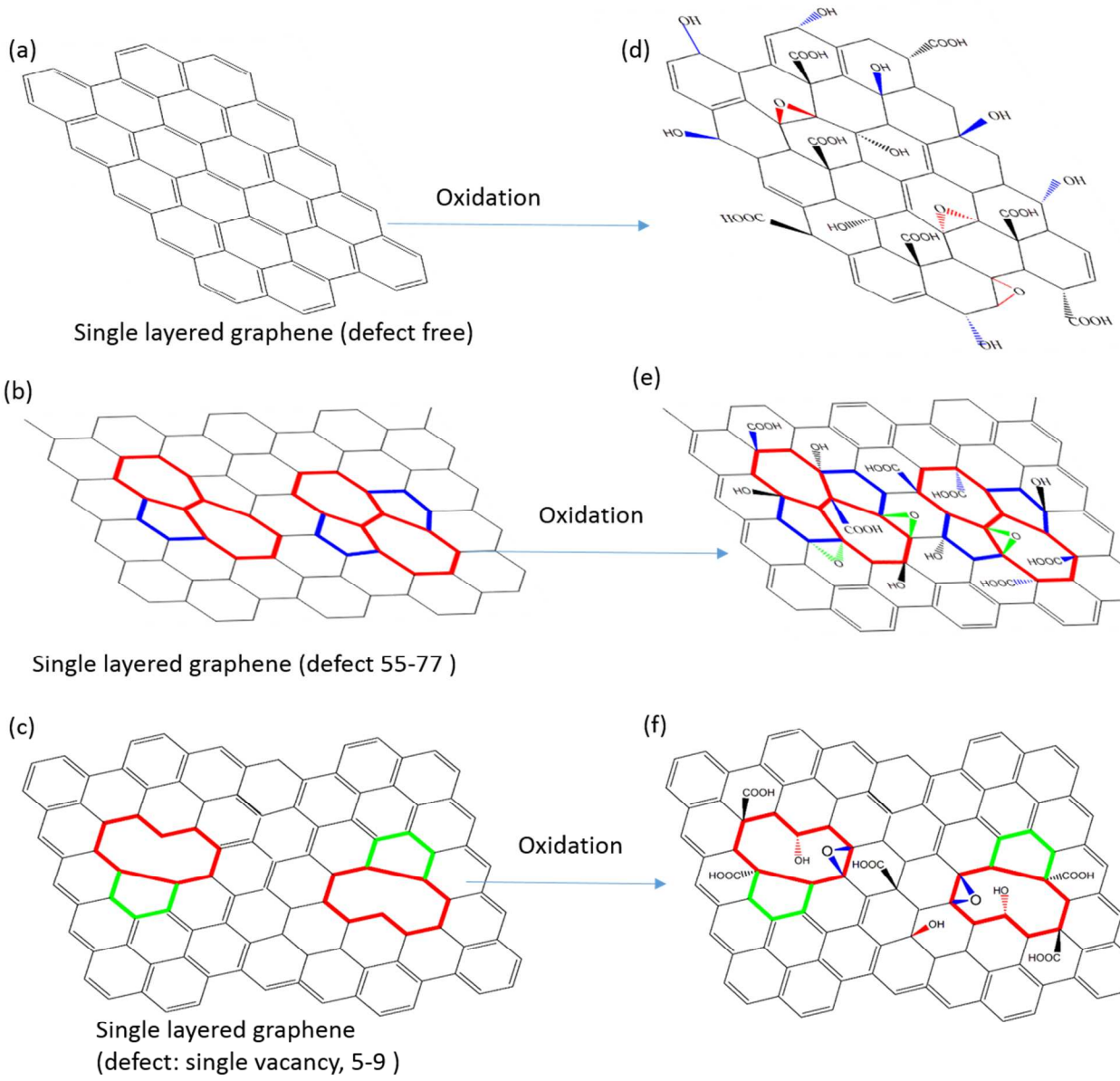

Figure 13.Schematic showing the single layered graphene, (a) defect free, (b) with 55-77 types of defect and (c) with defect single vacancy 5-9 type; (d), (e) and (f) are their oxidized forms, respectively.

Cite this: DOI: 10.1039/c0xx00000x

www.rsc.org/xxxxxx

ARTICLE TYPE

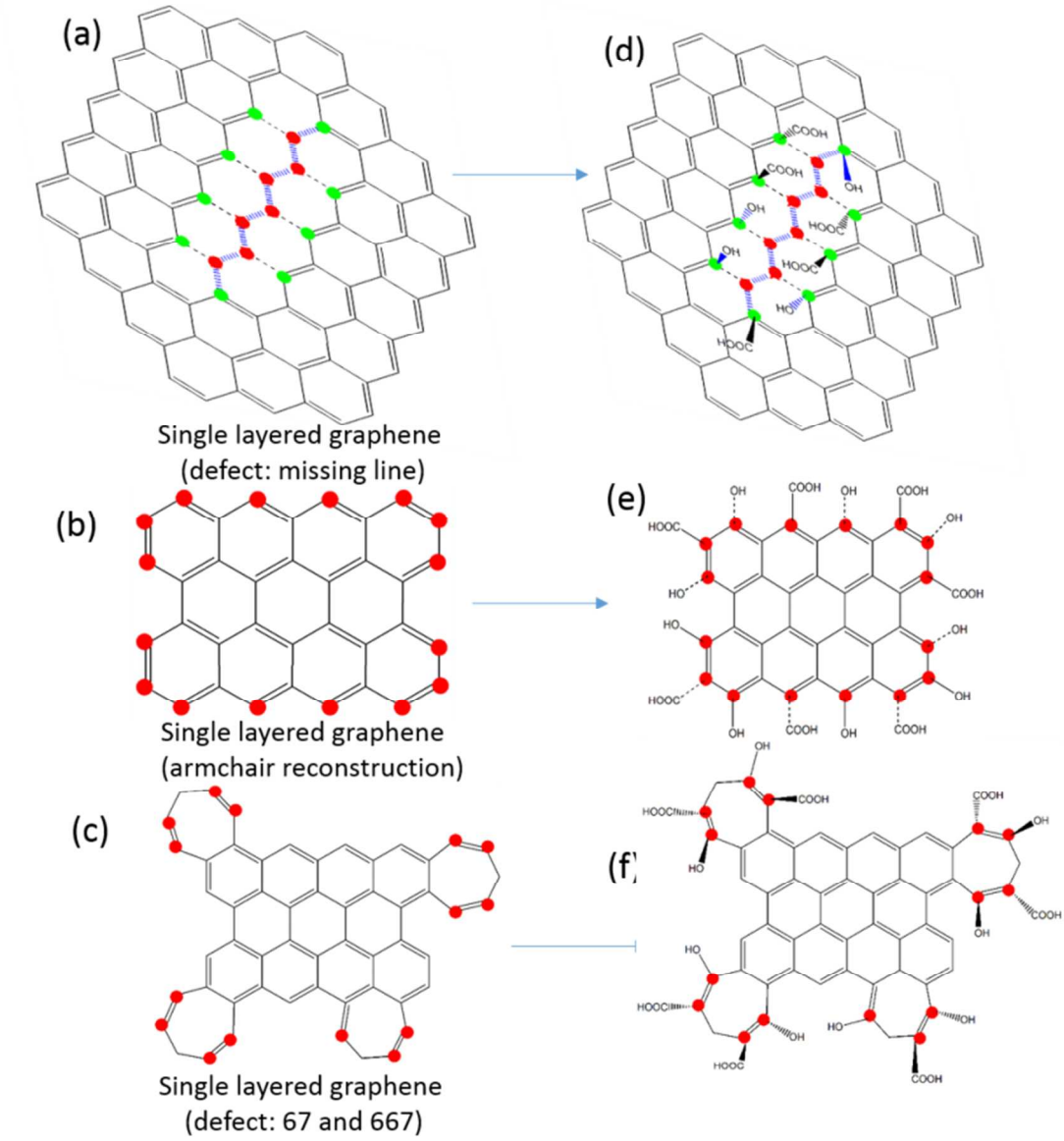

Figure 14. Schematic showing the single layered graphene, (a) with line defect (b) with armchair reconstructed form and (c) with defect 67 and 667 type; (d), (e) and (f) are their oxidized forms, respectively.

Cite this: DOI: 10.1039/c0xx00000x

www.rsc.org/xxxxxx

ARTICLE TYPE

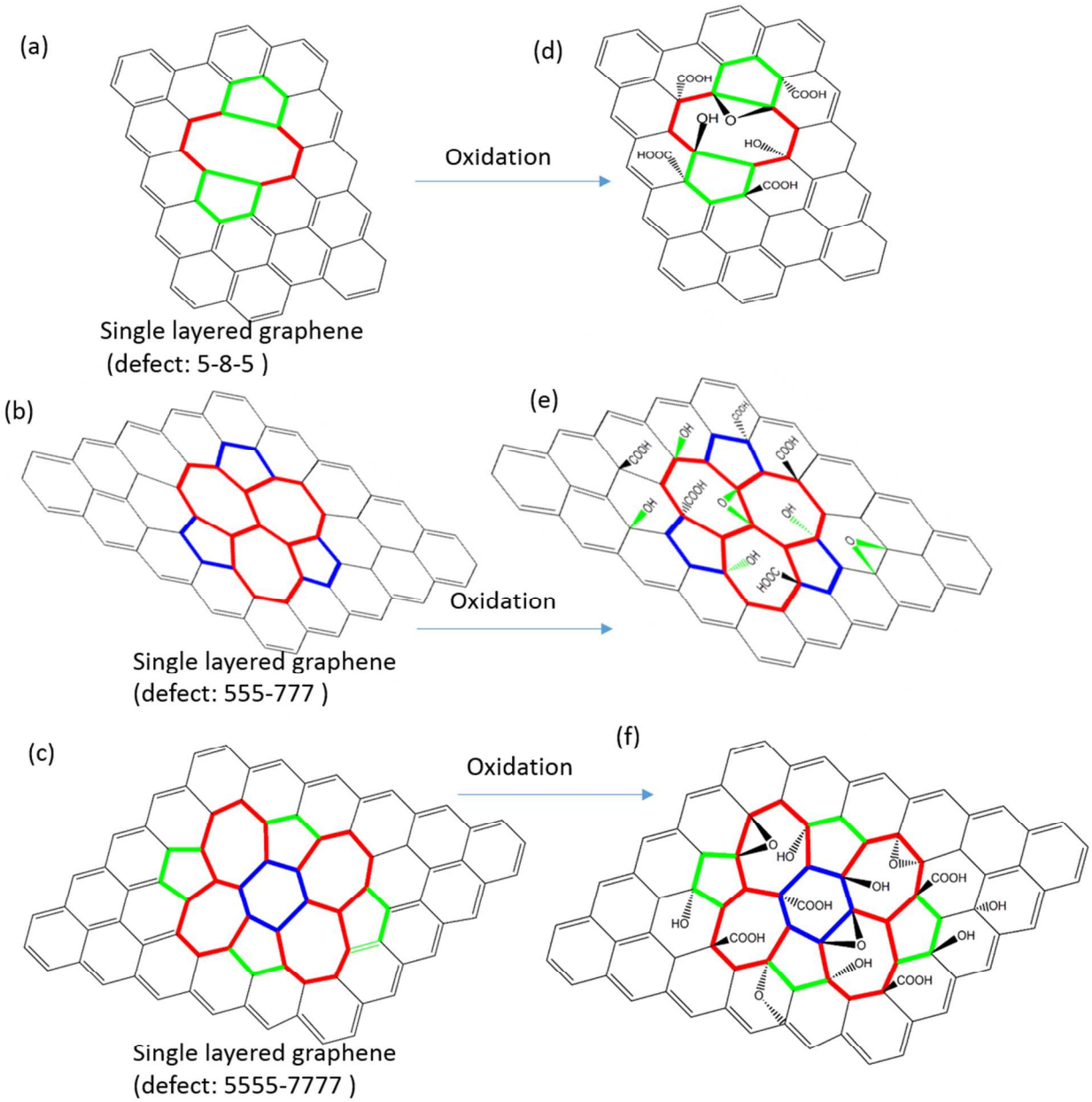

Figure 15. Schematic showing the single layered graphene, (a) defect type 5-8-5, (b) defect type 555-777 and (c) defect type 5555-7777; (d), (e) and (f) are their oxidized forms, respectively.

value is superior compared to the reported results for rGO/Cl-rGO/r-GO-polymer composites in the same frequency range.[24,53]Reduced graphene oxide have less number of oxygen containing functional groups and have very less dielectric constant values since it is conducting in nature and cannot be anticipated as an good insulator/dielectric material according to literature[54,55]. Further to study the role of the defects on dielectric constant of GO, we have performed a series of experiments and the results have been shown in supporting file (Figure S14), which revealed that the GO which has not sonicated during oxidation (GOL) has the less value for the dielectric constant in the same frequency range. Supporting Figure S15 is the evident for the less oxidation of GO (GOL).

4. Conclusions

In summary, a new single/few layered GO has been synthesized by modified Hammer's method and using sonochemical approach. A systematic investigation has been performed to study the dielectric behaviour of GO. Novel GO contains mainly –OH and –COOH functional groups which are responsible for the change in polarization of GO sheet under the applied electric fields at the various frequency and temperature range. Present study strongly concluded that the novel GO exhibits very high dielectric constant and is in the order of 10^6 in magnitude. This value is very high, which is even very high compared to the conventional giant dielectric material such as $CaCu_3Ti_4O_{12}$. The reorientation/rearrangement of the attached functional groups (-OH and -COOH) in the GO resulted change in the dipole moment and the polarization which lead to the high dielectric constant at low temperature and frequency range. The contribution of defects for the colossal dielectric value of GO also have been addressed. All the defects are very prone to chemical oxidation of single layered graphite/graphene. These defects cause to the restriction of л→л transition of electrons and give rise to the strong dipole at the defect sides and results an extraordinarily high value of dielectric constant with relatively low dielectric losses. This newly synthesized GO with colossal dielectric constant is likely to enable us further scaling advances in performances of the electronic and energy storage devices.

Notes and references

[a]*School of Engineering Sciences and Technology,and* [b]*Advanced Centre of Reseach in High Energy Materials, University of Hyderabad- 500046, Telangana, India. Tel: (+91)-(040) 2313 4457 (O); E-mail: pradip.paik@gmail.com, ppse@uohyd.ernet.in, paik@uohyd.ac.in*
[c]*School of Physics, University of Hyderabad- 500046, Telangana, India..*

† Electronic Supplementary Information (ESI) available: [Table S1 (a) Elemental analysis for GO, Figure S1: EDX spectra of Graphene oxide, Figure S2: Photographic image of GO pellet, Figure S3-S11: Cole-Cole plots of GO at various temperatures with fitted curves, Figure S12: TGA plot with derivative of grapite and Figure S13: TGA plotwith derivative of GO, Table S2: Elemental analysis for GOL, Figure S14 for dielectric results for GOL, Figure S15 EDX of GOL]. See DOI: 10.1039/b000000x/

References:

1. C. C. Homes and T. Vogt, *Nat Mater*, 2013, **12**, 782–783.
2. X. Hao, *J. Adv. Dielectr.*, 2013, **03**, 1330001.
3. H. Xu and L. Gao, *J. Am. Ceram. Soc.*, 2003, **86**, 203–205.
4. M. A. Subramanian, D. Li, N. Duan, B. A. Reisner, and A. W. Sleight, *J. Solid State Chem.*, 2000, **151**, 323–325.
5. A. P. Ramirez, M. A. Subramanian, M. Gardel, G. Blumberg, D. Li, T. Vogt, and S. M. Shapiro, *Solid State Commun.*, 2000, **115**, 217–220.
6. C. C. Homes, T. Vogt, S. M. Shapiro, S. Wakimoto, and A. P. Ramirez, *Science (80-.).*, 2001, **293**, 673–676.
7. S.-Y. Chung, I.-D. Kim, and S.-J. L. Kang, *Nat Mater*, 2004, **3**, 774–778.
8. L. He, J. B. Neaton, M. H. Cohen, D. Vanderbilt, and C. C. Homes, *Phys. Rev. B*, 2002, **65**, 214112.
9. L. He, J. B. Neaton, D. Vanderbilt, and M. H. Cohen, *Phys. Rev. B*, 2003, **67**, 12103.
10. C. C. Homes, T. Vogt, S. M. Shapiro, S. Wakimoto, M. A. Subramanian, and A. P. Ramirez, *Phys. Rev. B*, 2003, **67**, 92106.
11. D. C. Sinclair, T. B. Adams, F. D. Morrison, and A. R. West, *Appl. Phys. Lett.*, 2002, **80**, 2153–2155.
12. T. B. Adams, D. C. Sinclair, and A. R. West, *Adv. Mater.*, 2002, **14**, 1321–1323.
13. W. Si, E. M. Cruz, P. D. Johnson, P. W. Barnes, P. Woodward, and A. P. Ramirez, *Appl. Phys. Lett.*, 2002, **81**, 2056–2058.
14. L. Chen, C. L. Chen, Y. Lin, Y. B. Chen, X. H. Chen, R. P. Bontchev, C. Y. Park, and A. J. Jacobson, *Appl. Phys. Lett.*, 2003, **82**, 2317–2319.
15. W. Hu, Y. Liu, R. L. Withers, T. J. Frankcombe, L. Norén, A. Snashall, M. Kitchin, P. Smith, B. Gong, H. Chen, J. Schiemer, F. Brink, and J. Wong-Leung, *Nat Mater*, 2013, **12**, 821–826.
16. D. R. Dreyer, S. Park, C. W. Bielawski, and R. S. Ruoff, *Chem. Soc. Rev.*, 2010, **39**, 228–240.
17. H. He, J. Klinowski, M. Forster, and A. Lerf, *Chem. Phys. Lett.*, 1998, **287**, 53–56.
18. C. Gómez-Navarro, R. T. Weitz, A. M. Bittner, M. Scolari, A. Mews, M. Burghard, and K. Kern, *Nano Lett.*, 2007, **7**, 3499–3503.
19. H. Chen, M. B. Müller, K. J. Gilmore, G. G. Wallace, and D. Li, *Adv. Mater.*, 2008, **20**, 3557–3561.
20. Y. Bai, Y. Cao, J. Zhang, M. Wang, R. Li, P. Wang, S. M. Zakeeruddin, and M. Gratzel, *Nat Mater*, 2008, **7**, 626–630.
21. RamanathanT., A. A., StankovichS., D. A., Herrera-AlonsoM., P. D., A. H., S. C., ChenX., R. S., N. T., A. A., P. K., and B. C., *Nat Nano*, 2008, **3**, 327–331.
22. S. Stankovich, D. A. Dikin, G. H. B. Dommett, K. M. Kohlhaas, E. J. Zimney, E. A. Stach, R. D. Piner, S. T. Nguyen, and R. S. Ruoff, *Nature*, 2006, **442**, 282–286.
23. T. K. Gupta, B. P. Singh, V. N. Singh, S. Teotia, A. P. Singh, I. Elizabeth, S. R. Dhakate, S. K. Dhawan, and R. B. Mathur, *J. Mater. Chem. A*, 2014, **2**, 4256–4263.
24. J.-Y. Kim, W. H. Lee, J. W. Suk, J. R. Potts, H. Chou, I. N. Kholmanov, R. D. Piner, J. Lee, D. Akinwande, and R. S. Ruoff, *Adv. Mater.*, 2013, **25**, 2308–2313.
25. J.-Y. Wang, S.-Y. Yang, Y.-L. Huang, H.-W. Tien, W.-K. Chin, and C.-C. M. Ma, *J. Mater. Chem.*, 2011, **21**, 13569–13575.
26. L. J. Romasanta, M. Hernández, M. a López-Manchado, and R. Verdejo, *Nanoscale Res. Lett.*, 2011, **6**, 508.
27. P. Fan, L. Wang, J. Yang, F. Chen, and M. Zhong, *Nanotechnology*, 2012, **23**, 365702.
28. N. R. Wilson, P. A. Pandey, R. Beanland, R. J. Young, I. A. Kinloch, L. Gong, Z. Liu, K. Suenaga, J. P. Rourke, S. J. York, and J. Sloan, *ACS Nano*, 2009, **3**, 2547–2556.
29. F. Tuinstra, *J. Chem. Phys.*, 1970, **53**, 1126.
30. a. Ferrari and J. Robertson, *Phys. Rev. B*, 2000, **61**, 14095–14107.
31. S. Stankovich, D. a. Dikin, R. D. Piner, K. a. Kohlhaas, A. Kleinhammes, Y. Jia, Y. Wu, S. T. Nguyen, and R. S. Ruoff, *Carbon N. Y.*, 2007, **45**, 1558–1565.
32. S. Some, Y. Kim, E. Hwang, H. Yoo, and H. Lee, *Chem. Commun.*, 2012, **48**, 7732–7734.
33. D. Yang, A. Velamakanni, G. Bozoklu, S. Park, M. Stoller, R. D. Piner, S. Stankovich, I. Jung, D. A. Field, C. A. V. Jr., and R. S. Ruoff, *Carbon N. Y.*, 2009, **47**, 145–152.
34. J. Gass, P. Poddar, J. Almand, S. Srinath, and H. Srikanth, *Adv. Funct. Mater.*, 2006, **16**, 71–75.
35. P. Suresh and S. Srinath, *J. Alloys Compd.*, 2013, **554**, 271–276.

36. F. Banhart, J. Kotakoski, and A. V Krasheninnikov, *ACS Nano*, 2011, **5**, 26–41.
37. A. Lherbier, S. M.-M. Dubois, X. Declerck, Y.-M. Niquet, S. Roche, and J.-C. Charlier, *Phys. Rev. B*, 2012, **86**, 75402.
38. A. Sendilkumar, K. C. J. Raju, P. D. Babu, and S. Srinath, *J. Alloys Compd.*, 2013, **561**, 174–179.
39. A. Lerf, H. He, M. Forster, and J. Klinowski, *J. Phys. Chem. B*, 1998, **102**, 4477–4482.
40. D. W. Boukhvalov and M. I. Katsnelson, *Nano Lett.*, 2008, **8**, 4373–4379.
41. G. Cantele, Y.-S. Lee, D. Ninno, and N. Marzari, *Nano Lett.*, 2009, **9**, 3425–3429.
42. X. Peng and R. Ahuja, *Nano Lett.*, 2008, **8**, 4464–4468.
43. E. J. Duplock, M. Scheffler, and P. J. D. Lindan, *Phys. Rev. Lett.*, 2004, **92**, 225502.
44. F. Banhart, J. Kotakoski, and A. V Krasheninnikov, *ACS Nano*, 2011, **5**, 26–41.
45. A. J. Stone and D. J. Wales, *Chem. Phys. Lett.*, 1986, **128**, 501–503.
46. L. Li, S. Reich, and J. Robertson, *Phys. Rev. B*, 2005, **72**, 184109.
47. J. Ma, D. Alfè, A. Michaelides, and E. Wang, *Phys. Rev. B*, 2009, **80**, 33407.
48. A. V Krasheninnikov, P. O. Lehtinen, A. S. Foster, and R. M. Nieminen, *Chem. Phys. Lett.*, 2006, **418**, 132–136.
49. A. A. El-Barbary, R. H. Telling, C. P. Ewels, M. I. Heggie, and P. R. Briddon, *Phys. Rev. B*, 2003, **68**, 144107.
50. M. H. Gass, U. Bangert, A. L. Bleloch, P. Wang, R. R. Nair, and G. K., *Nat Nano*, 2008, **3**, 676–681.
51. J. C. Meyer, C. Kisielowski, R. Erni, M. D. Rossell, M. F. Crommie, and A. Zettl, *Nano Lett.*, 2008, **8**, 3582–3586.
52. R. H. Telling, C. P. Ewels, A. A. El-Barbary, and M. I. Heggie, *Nat Mater*, 2003, **2**, 333–337.
53. D. Wang, X. Zhang, J.-W. Zha, J. Zhao, Z.-M. Dang, and G.-H. Hu, *Polymer (Guildf).*, 2013, **54**, 1916–1922.
54. I. Jung, D. A. Dikin, R. D. Piner, and R. S. Ruoff, *Nano Lett.*, 2008, **8**, 4283–4287.
55. H. Liu, L. Zhang, Y. Guo, C. Cheng, L. Yang, L. Jiang, G. Yu, W. Hu, Y. Liu, and D. Zhu, *J. Mater. Chem. C*, 2013, **1**, 3104–3109.

Graphical Abstract